2015 Tenth International Conference on Ecological Vehicles and Renewable Energies (EVER)

Multi-Objective Optimization of In-Wheel Motor Powertrain and Validation Using Vehicle Simulator

Kesavan Ramakrishnan, Massimiliano Gobbi, Gianpiero Mastinu
Department of Mechanical Engineering
Politecnico di Milano (Technical University)
Piazza Leonardo da Vinci 32, 20133 Milan, Italy
Email:kesavan.ramakrishnan@polimi.it

***Abstract*—A method based on multi-objective optimization (MOO) is employed for the concept design of electric powertrain with in-wheel motor (IWM). The inherent challenges of IWM vehicles are powertrain packaging, increased unsprung mass, and motor cooling. Elimination of hub-reduction gearbox and adaption of high torque and low power electric motor can mitigate these challenges, but it degrades high speed gradeability. Simultaneous optimization of motor power, battery size and drivability parameters to size the powertrain components (electric motor and gearbox) is important for the effective design of powertrain layout. In this study, motor torque, base speed, and gear-ratio are taken as design variables to minimize the motor peak power and the battery size, while maximizing the drivability performance. AC induction machines and Li-ion batteries are considered for the discussion, but the same approach can be applied for other motor and battery types. The results are validated virtually using a high-fidelity vehicle simulator, which confirms the findings of MOO. The optimal powertrain layout includes a high torque (600Nm) and low speed motor without gearbox.**

***Keywords*—In-wheel motor; Pareto optimization; virtual validation; Willans approach.**

NOMENCLATURE

m_v	Vehicle mass (kg)
C_d	Drag coefficient
A	Frontal area of the vehicle (m^2)
ρ	Density of Air (kg/m^3)
V	Vehicle velocity (m/s)
C_r	Coefficient of rolling resistance
θ	Gradient (rad)
g	Gravity (m/s^2)
a	Vehicle acceleration (m/s^2)
SOC	Battery state of charge (%)
GR	Gear ratio
T_{em}	Electric torque curve (Nm)
T_{peak}	Motor peak torque(Nm)
ω_{em}	Rotational speed (rad/s)
ω_{BS}	Base speed (rad/s)
η_{em}	Motor efficiency (%)
P_{peak}	Motor peak power (kW)
P_{acc}	Acceleration power requirement (kW)
P_{maxvel}	Max velocity power requirement (kW)
P_{grad}	Gradeability power requirement (kW)
P_{dc}	Driving cycles power requirement (kW)
P_{op}	Motor output power (kW)
P_{in}	Motor input electric power (kW)
P_{loss}	Motor & Power electronics losses (kW)
e_{int}	Intrinsic efficiency (%)
r, l	rotor radius and length (m)
η_{rec}	Recuperation efficiency (%)
NBC	Number of battery cells
m_c	Effective heat capacity per cell ($J/°C$)
hA	Convective heat transfer ($W/°C$)
T_{batt}	Battery temperature ($°C$)
T_{amb}	Atmosphere temperature ($°C$)
E_{NEDC}	Energy requirement of NEDC (kJ)
E_{range}	Energy requirement of range target (kJ)

I. INTRODUCTION

According to WHO report [1], urban population in 2014 is 54% of total global population, this figure is expected to grow up to 66% by 2050. Vehicles are also growing in number in the urban regions, which exacerbate the problems on atmospheric pollution and greenhouse gas concentration. Traffic congestion is another major issue that requires immediate attention from the automakers. In Moscow, which has the worst peak hour index [2], an average 30 minute trip in free flow conditions takes 68 minutes during peak hours. Therefore the urban vehicles should be made compact in addition to being energy efficient.

The idea of in-wheel motor with a hub reduction planetary gear sets was first conceived by Wellington Adams [3] in 1884. Albert Parcelle [4] in 1890 eliminated the gearbox and directly mounted a motor on the wheel. In the same time Edward Parkhurst [5] has invented a

978-1-4673-6785-1/15/$31.00

high torque low speed motor by arranging two radial field magnet sets in series along the rotor axis, which was an appropriate solution for this application. Lohner-Porsche was the first vehicle designed by Ferdinand Porsche to have in-wheel motors, it was presented at the Paris motor show in 1900. Thereafter many concept vehicles from different OEMs have proven that IWM is a viable powertrain option. Some of the concept vehicles are ZAP-x, Peugeot BB1, Ford F-150 (powered by Protean Electric motor), Hiriko folding electric car, Volvo ReCharge, Ford Fiesta E-Wheel Drive, and Nissan BladeGlider. Though these vehicles have not yet been put into production, it is evident that the auto industry is strongly considering IWM as a potential future mobility solution.

This paper presents a methodology to optimally select in-wheel motor powertrain (IMW) components based on multiple objective functions and constraints, it also proposes virtual validation using a vehicle simulator. The discussion first focuses on the mathematical model of electric powertrain and then the computation of Pareto-optimal set. Multi-objective optimization (MOO) was first applied by exploiting computer simulations in economics to solve public investment problems in 1960s [6]. From that time onwards the technique had many applications in the engineering field. Buerger, S [7] used this technique for the optimization of hybrid vehicles component-sizes as well as control strategies, he also quantified the trade-off between solutions. Robert Cook et al. [8] optimized drivetrain and driving strategies as per multiple design objectives. But sometimes Pareto-optimal set is too large for the designers to consider and choose one solution from them. k and k-ϵ optimality selection approach proposed by Gobbi [9] can be used to rank the Pareto solutions and to make a selection based on this rankings. Validation of the final selection is another concern in the optimization process. X.D Xue et al. [10] employed multi-objective optimization for IWM vehicle application and validated the results using a physical prototype, which is an expensive and time consuming method. In many research papers vehicle simulators have been discussed and their results are proven to be accurate enough to replace early stage prototypes [11]. Such a soft validation method is proposed and the key aspects of building such simulator are explained.

Section-II explains electric motor and energy consumption models. In Section-III, multi-objective optimization is introduced and the objective functions are formulated in section-IV. Optimal solutions are derived in section-V, which are validated using a simulator elaborated in section-VI. The results and future work are presented in section VII and VIII.

II. POWERTRAIN MODEL

The powertrain consists of IWM (either with or without reduction gearbox), power electronics and battery pack. Power electronic unit is included in the motor for simplicity and the combined efficiency map is used for calculations.

A. Electric motor model

Motor torque and power curves are formulated as given in (1, 2). They are divided into constant torque ($\omega_{em} \leq \omega_{BS}$) and constant power ($\omega_{em} > \omega_{BS}$) sub-regions.

$$T_{em} = \begin{cases} T_{peak}, & \omega_{em} \leq \omega_{BS} \\ \frac{T_{peak}\omega_{BS}}{\omega_{em}}, & \omega_{em} > \omega_{BS} \end{cases} \quad (1)$$

$$P_{em} = \begin{cases} T_{peak}\omega_{em}, & \omega_{em} \leq \omega_{BS} \\ T_{em}\omega_{em}, & \omega_{em} > \omega_{BS} \end{cases} \quad (2)$$

Motor efficiency map is modelled using Willans approach [12], which can be converted into a scalable model by normalizing torque and speed in analogy to what is done for IC engines. This model allows to find the operating efficiencies of different motor sizes that are considered for optimization study. A three phase AC induction machine efficiency map, taken from MOTOR-CAD model, is considered for the calculation. At each operating speed, input and output powers are represented as an affine function defined in (3). Intrinsic energy conversion efficiency (e_{int}) and motor losses after energy conversion (P_{loss}) are obtained from curve fitting.

$$P_{op} = e_{int}P_{in} - P_{loss} \quad (3)$$

Mean effective pressure (p_{me}) is defined as a ratio between tangential force acting on the rotor periphery and its surface area.

$$p_{me} = \frac{T_{em}}{r2\pi rl} = \frac{T_{em}}{2V_r} = \frac{P_{op}}{2V_r\omega_{em}} \quad (4)$$

Similarly the mean available pressure (p_{ma}), mean loss pressure (p_{ml}), and mean tangential speed of the rotor (C_m) are defined in the equations below.

$$p_{ma} = \frac{P_{in}}{2V_r\omega_{em}} \quad (5)$$

$$p_{ml} = \frac{P_{loss}}{2V_r\omega_{em}} \quad (6)$$

$$C_m = r\omega_{em} \quad (7)$$

Therefore, (3) can be rewritten in the form of normalized variables as,

$$p_{me} = e_{int}p_{ma} - p_{ml} \quad (8)$$

Intrinsic efficiency (e_{int}) and mean loss pressure (p_{ml}) are approximated as fourth order polynomial functions of C_m using curve fitting method.

$$e_{int} = \sum_{i=0}^{4} e_{inti} C_{mi} \tag{9}$$

$$p_{ml} = \sum_{i=0}^{4} p_{mli} C_{mi} \tag{10}$$

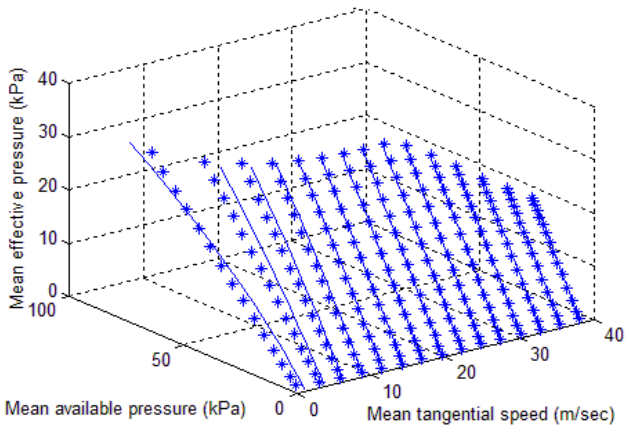

Fig. 1. Willans line model.

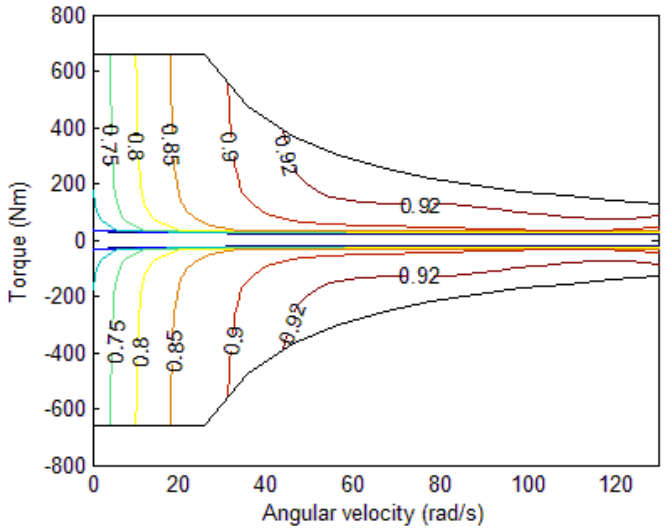

Fig. 2. Efficiency map.

Based on these equations, rotor sizes (radius-r and length-l) are changed to scale the motor size without altering the normalized parameters. Fig.1 shows Willans line model of a 20 kW electric machine (dotted lines) scaled from a 66 kW machine (solid line) and Fig.2 shows an equivalent efficiency map. Using this scaled map, operating efficiencies of the motor can be derived at each of torque and speed combinations. This method of scaling is restricted to the same family of electric motor considered.

B. Energy consumption model

Electrical energy required from the battery is calculated by integrating tractive power and powertrain loss at every instance. The graphs below show New European Driving Cycle (NEDC) [13] driving cycle and its instantaneous power demand calculated for the vehicle parameters given in Table I. Motor losses are obtained from Willans line model. A fixed drivetrain loss is included, when hub-reduction gearbox is present. Auxiliary power requirements are not included.

Integration of the positive powers(11), shown in Fig.3, gives energy demand without any recuperation. Similar integration of negative powers(12) gives available energy for possible recuperation. Service brake is applied based on driving situations that dissipates the kinetic energy into heat. Natural braking (rolling resistance and air drag) always acts against the vehicle direction. Hence, only a portion of the available negative energy can be recuperated.

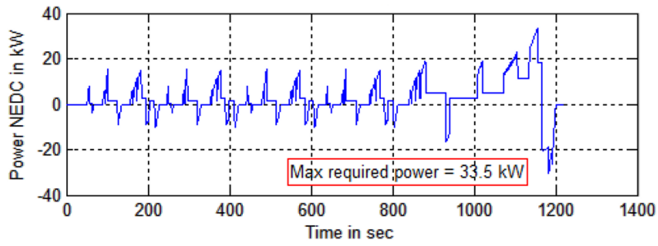

(a) Velocity profile

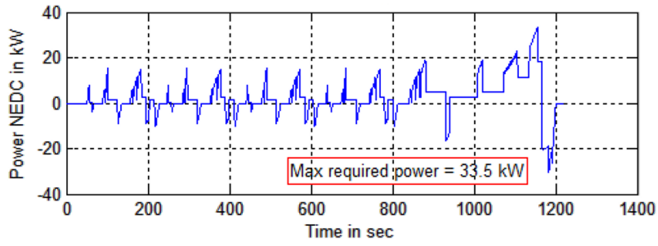

(b) Power demand

Fig. 3. NEDC driving cycle

$$E_{positive.NEDC} = \int P_{positive} \mathrm{d}t \tag{11}$$

$$E_{negative.NEDC} = \int P_{negative} \mathrm{d}t \tag{12}$$

$$E_{NEDC} = E_{positive.NEDC} + \eta_{rec} E_{negative.NEDC} \tag{13}$$

$$E_{range} = \frac{E_{NEDC}}{D_{NEDC}} Range \tag{14}$$

A simplified battery model is employed, which assumes constant terminal voltage and recuperation efficiency (η_{rec}). Considering all-wheel drive powertrain (higher total regenerative torque) and the battery size

(higher charging rate), the average recuperation efficiency(13) can be assumed as 70%. Battery capacity requirement as per NEDC driving cycle is calculated for the desired range target using (14).

TABLE I. VEHICLE PARAMETERS

S.NO	Parameters	Target	Units
1	Vehicle body mass+driver	1000+75	kg
2	Powertrain mass	Depends on motor peak power and battery size	kg
3	Frontal Area, A	2	m^2
4	Co-efficient of drag, C_d	0.3	-
5	Center of gravity height	550	mm
6	Wheel base	2600	mm
7	Maximum speed	150	km/h
8	Range	160	km
9	Static weight distribution	50:50	%

III. MULTI OBJECTIVE OPTIMIZATION

The component sizing optimization problem of IWM powertrain is formulated as a classical MOO problem [14], [15],

$$\min[f(x)] \quad (15)$$
$$x \epsilon S$$
$$S = \{x \epsilon R^m : H(x) = 0, G(x) \geq 0\}$$

Where, f is an objective function vector, x is a design variable vector, and S includes both equality and inequality constraints.

TABLE II. OPTIMIZATION PROBLEM FORMULATION

Design variables	T_{peak}, ω_{BS}, GR
Objective functions	min(P_{peak},NBC,$inv(Gradeabiliy)$)
Constraints	Acceleration(m/s^2) $\epsilon[a_{min}, a_{max}]$=[2.78, 9.81]
	Acceleration time(sec)$\epsilon[t_{min}, t_{max}]$=[3,10]
	Maximum speed (km/h) = V_{max}= 160
	Gear ratio $\epsilon[GR_{min}, GR_{max}]$ = [1, 8]
	$P_{peak} \geq max(P_{acc}, P_{max.vel}, P_{grad}, P_{dc})$
	Torque (Nm) ϵ $[T_{min}, T_{max}]$ = [50, 800]
	SOC (%) ϵ $[SOC_{min}, SOC_{max}]$ = [20, 90]

In this design problem, motor peak power (P_{peak}), gradeability, and battery size (NBC) are the function to be optimized. Among these functions, motor peak power and battery size should be minimized to keep the vehicle weight and cost down. On the other hand gradeability that represents vehicle performance has to be maximized. In order to have common optimization goal, inverse of Gradeability (inv(Gradeability)) is taken as an objective function. They are modelled as functions of design variables, such as motor peak torque (T_{peak}), base speed (ω_{BS}), and gear-ratio (GR). Performance requirements on maximum speed and acceleration time are defined as constraints.

IV. OBJECTIVE FUNCTIONS FORMULATION

A. Motor Peak Power

Motor peak power should satisfy the power demands from different vehicle requirements including acceleration (P_{acc}), maximum velocity ($P_{max.vel}$), driving cycles (P_{dc}), and legislative targets on gradeability (P_{grad}).

$$P_{peak} = T_{peak}\omega_{BS} \geq \max(P_{acc}, P_{max.vel}, P_{grad}, P_{dc}) \quad (16)$$

Among these requirements, P_{acc} is the dominant value and it depends on vehicle acceleration profile, which will be explained in detail below.

1) Acceleration: Fig.4 shows multiple ways [16] to achieve the acceleration requirement of 0-100kmph in 10 sec. When the acceleration is kept maximum (traction limit - 9.81 m/s^2) at lower speeds and reduced hyperbolically at higher speeds, the motor power requirement is less than having constant acceleration across the speed range. But the torque at the wheel needs to be increased to achieve high initial acceleration. The same can be obtained either by increasing motor torque or by introducing hub reduction gearbox.

$$P_{acc} = m_v a V + m_v C_r V + \frac{1}{2} C_d \rho A V^3 \quad (17)$$

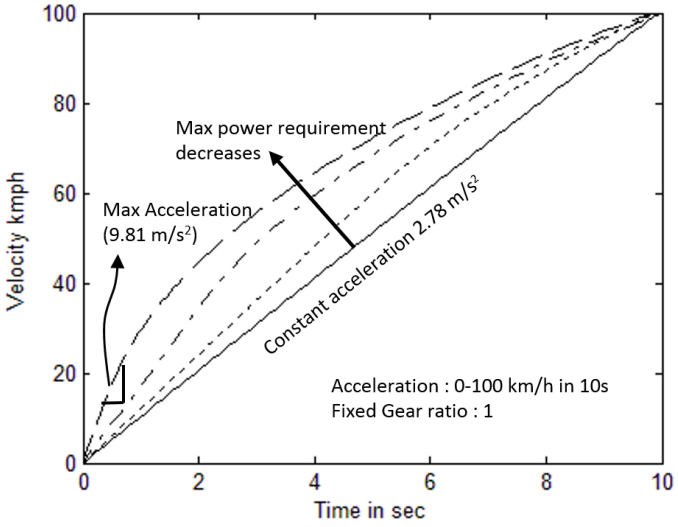

Fig. 4. Acceleration performance.

Gradient force is not included in (17) with an assumption that the maximum acceleration is targeted on flat road condition. Slip [11] at the driving wheel is neglected up to traction limit. Tire rolling resistance coefficient [17] is modelled as a function of vehicle velocity.

$$C_r = 0.005 + 10^{-7} V^{2.5} \quad (18)$$

2) Driving cycle, Maximum velocity, and gradeability: ARTEMIS (urban, motorway, and combined) and NEDC are considered. The tractive power is calculated by substituting velocity profile and vehicle parameters in (19). P_{maxvel} and P_{grad} are also calculated using the same equation. P_{grad} is the power needed to meet legislative requirements on gradeability at different speeds.

$$\begin{pmatrix} P_{dc} \\ P_{grad} \\ P_{maxvel} \end{pmatrix} = m_v V(a+g\sin(\theta)+C_r\cos(\theta))+\frac{1}{2}C_d\rho AV^3 \tag{19}$$

B. Battery size

Power demand from the inverter and the electric energy requirement calculated from (14) are the governing factors of battery size.

$$NBC = \max(NBC_{power}, NBC_{energy}) \tag{20}$$

where,

$$NBC_{power} = \frac{P_{in}}{Cellpower(kW)}$$

$$NBC_{energy} = \frac{E_{NEDC}}{70\%Cellcapacity(kJ)}$$

Li-ion prismatic battery cell with 19.5Ah capacity, 3.3V terminal voltage, and 400W discharge power is used for this study. Useful energy of the battery is taken as 70% (90% to 20%) of its capacity.

C. Gradeability

Gradeability [17] is defined as the maximum grade angle that the vehicle can overcome in the whole speed range. It can also be thought as available tractive force at different speeds on a flat road. Two motor power ratings, which have the same acceleration performances (0-100kmph in 10sec), are compared in Fig.5. They are observed to have different high speed gradeability values. Condition-1 corresponds to low power demand (68kW), where torque is high initially and then deceases hyperbolically as speed increases. Condition-2 has constant acceleration throughout the speed range that results in better high speed gradeabillity with higher power demand (128.6kW). Gradeability is calculated (21) at 100kmph for optimization purpose.

$$\sin(\theta) = \frac{d - C_r^2\sqrt{1-d^2+C_r^2}}{1+C_r^2} \tag{21}$$

$$d = \frac{\frac{P_{op}}{V} - \frac{1}{2}C_d\rho AV^2}{mg}$$

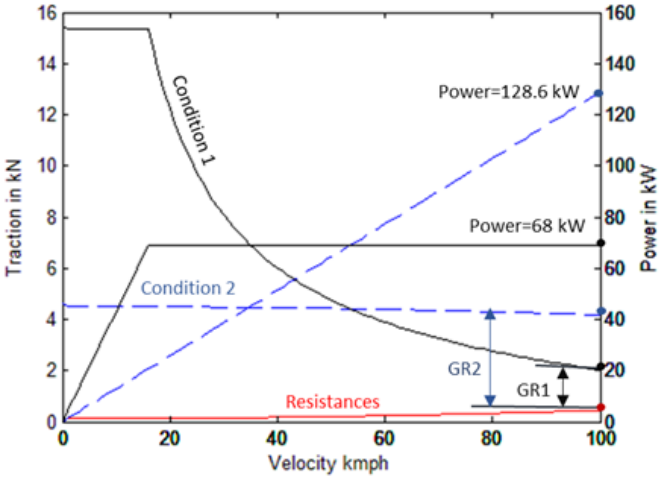

Fig. 5. Gradeability comparison.

V. GLOBAL SENSITIVITY ANALYSIS AND PARETO OPTIMAL SET

Global sensitivity analysis (GSA) describes the relationships between objective functions in the whole feasible design variable domain. Spearman rank correlation coefficient (r_s) method [18] is employed here. The values of r_s vary between +1 and -1. Values close to +1 indicate strong direct correlation, values close to -1 indicate strong inverse correlations, and values close to 0 indicate the absence of correlation. It can be seen from Table III that there exists a strong positive (monotonically increasing) correlation between the two objective functions, motor peak power and number of battery cells, so one of these objective functions can be eliminated in order to reduce the computational effort in the subsequent optimization process. The effect of removing one objective function on the final results will be studied and presented in this paper. A low discrepancy sequence (Sobol) [18] is used for design variable sampling as it provides high uniformity for efficient computation of Pareto-optimal set.

TABLE III. SPEARMAN RANK CORRELATION COEFFICIENTS

Objective functions	Correlation coefficient (r_s)
P_{peak} vs. NBC	0.9393
NBC vs. inv(Gradeability)	-0.9987
inv(Gradeability) vs. P_{peak}	-0.9240

A. Three Objective functions optimization

Pareto-optimal set, which is the best obtainable compromise between the conflicting objective functions, has been computed with all three functions and plotted Fig.6 in the objective function domain.

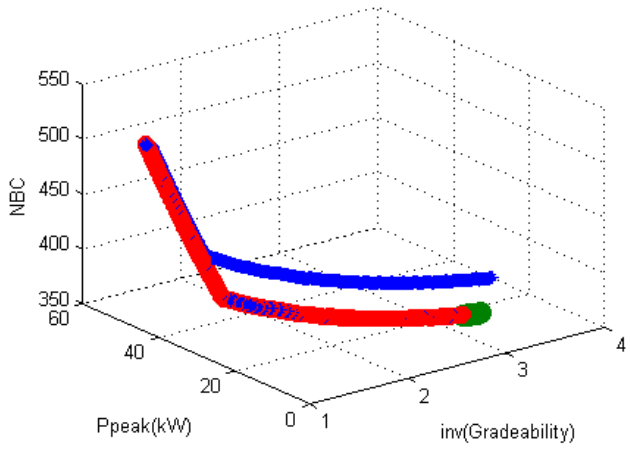

Fig. 6. Three Objective functions optimization.

B. *Two objective functions optimization*

Motor peak power has been eliminated and the optimization process is performed with NBC and inv(Gradability). The results are shown in Fig.7.

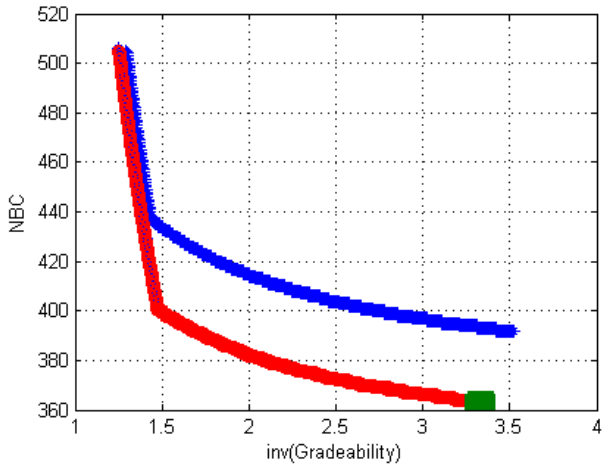

Fig. 7. Two Objective functions optimization.

It is evident from Fig.6,7 that the elimination of one objective function based on spearman rank correlation coefficient analysis (r_s) doesn't change the final results. The Pareto-optimal set in design variable domain remains unchanged as shown in Fig.8.

Decision makers can select one of the Pareto-optimal solutions based on their preferences. Target market, customer needs, part availability, and many more things can influence the final selection in a real situation. In this study, selection is made by prioritizing the objective functions. Higher priority is given to NBC (20) as the vehicle is targeted to be energy efficient. In the above Fig.6,7,8, Blue colored points indicate feasible domain,

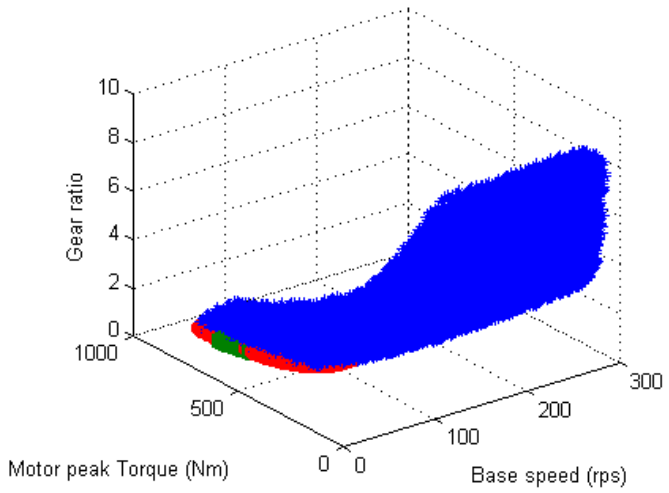

Fig. 8. Design Variables.

red colored points show Pareto-optimal set, and the green colored points correspond to minimum value of NBC. The final optimal solution for this problem is proposed in Table IV.

TABLE IV. OPTIMIZATION RESULTS

Optimum Specifications	Values
Motor torque	600 Nm
Base speed	28 rad/s
Motor power	16.2 kW
Gear ratio	1 (No gearbox)
Battery size	363 cell
Gradeability at 100kmph	9 degrees

VI. VEHICLE MODEL

A high-fidelity vehicle simulator [19], [20] that represents a complete electric vehicle is employed to validate the proposed solution. The simulator contains a PID driver control module, a detailed powertrain model, and a vehicle dynamics model. Based on desired velocity profile and current vehicle velocity, the PID controller estimates throttle and brake pedal positions, which are used to calculate electric motor and brake torque values. These torques are limited at multiple levels considering the operating conditions. In Fig.9, the demanded braking torque is shared between electric motor and service brake based on battery SOC and rate of change of brake pedal position. In case of panic braking condition or when the battery SOC is above a preset value, service brake is engaged to produce the desired braking torque, otherwise recuperation happens through the electric motor. As the maximum discharging and charging currents of the battery are limited for safety reasons, the motor demanded torque is restricted in both positive and negative directions.

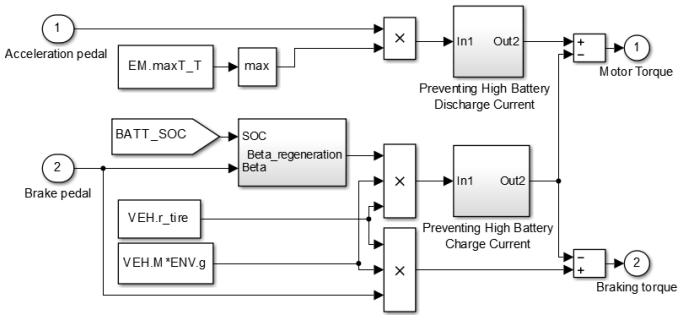

Fig. 9. Torque Management.

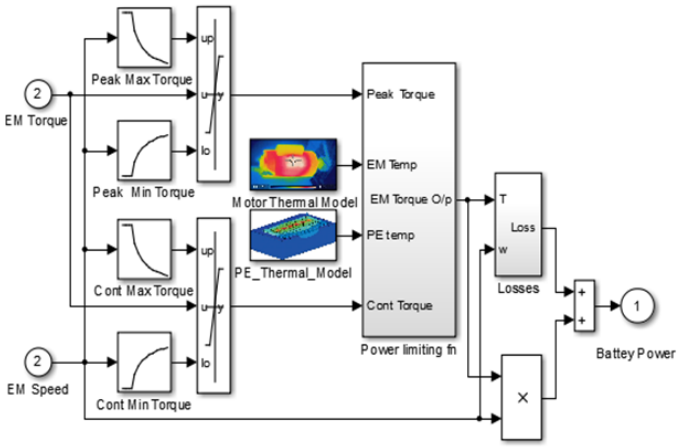

Fig. 10. Electric motor model.

Motor demanded torque is further restricted by torque vs. speed curves as in Fig.10. The motor is allowed to run above the continues max torque line only when operating temperatures of the motor and power electronic components are below an acceptable safe limits. Detailed thermal models [21], [22] calculate the temperatures of various components inside the motor and power electronics. As the rotor shaft is rigidly connected to the wheel, angular speed of the motor can be obtained from vehicle velocity directly. Instantaneous motor output power and powertrain losses are added together to get electric power demand from the battery. Integration of this instantaneous electric power over the range target gives battery capacity required.

Battery has been modelled as a first order equivalent circuit to capture the output voltage dynamic behaviour as shown in Fig.11.

$$V_b = E_0 - RI - V_c \tag{22}$$

$$\frac{dV_c}{dt} + \frac{1}{R_0 C_0} V_c = \frac{1}{C_0} \tag{23}$$

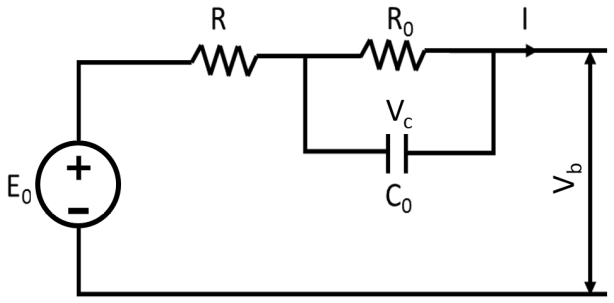

Fig. 11. Battery first order model.

Open circuit voltage (E_0), internal resistance (R), and RC circuit components (R_0, C) are modelled as quadratic functions of state of charge (SOC) and temperature (T_{batt}).

$$E_0 = \alpha_0 + \alpha_1 SOC + \alpha_2 SOC^2 + \alpha_3 T_{batt} + \alpha_4 SOC T_{batt} \tag{24}$$

$$R_1 = \beta_0 + \beta_1 SOC + \beta_2 SOC^2 + \beta_3 T_{batt} + \beta_4 SOC T_{batt} \tag{25}$$

$$R_2 = \beta_5 + \beta_6 SOC + \beta_7 SOC^2 + \beta_8 T_{batt} + \beta_9 SOC T_{batt} \tag{26}$$

$$C = \beta_{10} + \beta_{11} SOC + \beta_{12} T_{batt} \tag{27}$$

Battery SOC depends on current flow across the battery and its initial capacity, which is governed by Peukert's law [23].

$$SOC\% = SOC_0\% - \left(\int \frac{I}{C_I} dt \right) 100 \tag{28}$$

The simplified thermal model assumes the battery as a lumped mass, where heat addition and removal happen uniformly across all the cells.

$$m_c \frac{dT_{batt}}{dt} = RI^2 + R_0 I_{R0}^2 - hA(T_{batt} - T_{amb}) \tag{29}$$

Vehicle dynamics model in the simulator calculates acceleration, velocity, and distance from tractive force and road loads calculated as per (19) using the vehicle parameters given in Table I.

VII. SIMULATION RESULT

The vehicle simulator is used to calculate energy consumption over the range target and to verify drivability performance requirements including acceleration time, maximum speed, and gradeability. It eliminates the need for vehicle prototypes for preliminary evaluations in the early design phase. Optimum powertrain specifications shown in Table IV are considered for building the simulator and it is observed that the selected design variables are meeting the targets. Battery SOC profile over the targeted range as per NEDC driving cycle is given in

Fig.12. Initial SOC of the battery is 90% and it reaches to 20% after driving for 160km.

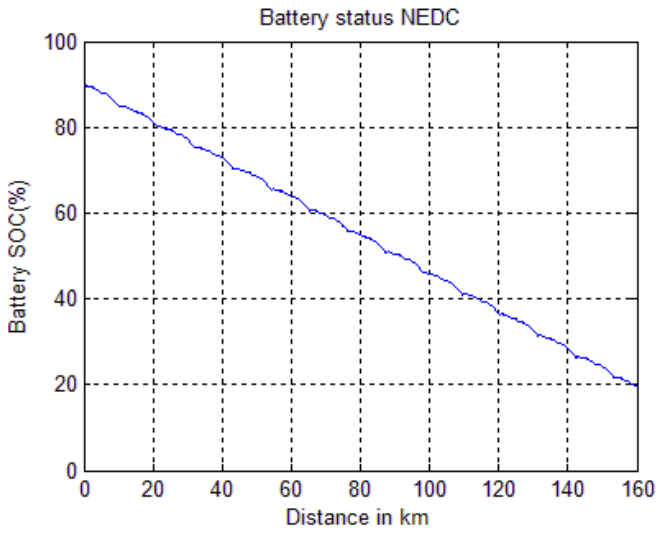

Fig. 12. Battery SOC profile.

VIII. CONCLUSION AND FUTURE WORK

In this paper, a two-step method for the concept design of electric powertrain has been presented. Initially the powertrain components are optimally selected using a multi-objective optimization procedure. In order to perform the optimization, the objective functions are mathematically modelled as functions of design variables. Their dependencies were checked using Spearman rank correlation coefficient and the Pareto-optimal set was computed. The final selection was made by prioritizing the objecting functions based on the designer?s preference. As a second step, the selected optimal solution was validated using a vehicle simulator built in MATLAB/SIMULINK environment. The results demonstrate that the proposed powertrain components have maximum powertrain efficiency with acceptable drivability performances. Elimination of the gearbox is optimal for the considered designer's preference, which will vary based on the vehicle type. For example, a high performance vehicle will require a gearbox to achieve better traction. Motor dimensions are not considered in this paper as they are strongly influenced by the motor topology, i.e. permanent magnet machines are having much better power density values compared to permanent-magnet-less machines.

The further work will be on optimization of electric motor parameters for the vehicle level objective functions specified here along with packaging constraints. This complex problem will be solved using analytical target cascading (ATC) [24] approach. The accuracy of validation simulator will be improved by co-simulating dedicated software for each sub-systems.

ACKNOWLEDGMENT

This paper is part of the ADvanced Electric Powertrain Technology (ADEPT) project which is an EU funded Marie Curie ITN project, grant number 607361. Within ADEPT a virtual and hardware tool are created to assist the design and analysis of future electric propulsions. Especially within the context of the paradigm shift from fuel powered combustion engines to alternative energy sources (e.g. fuel cells, solar cells, and batteries) in vehicles like motorbikes, cars, trucks, boats, planes. The design of these high performance, low cost and clean propulsion systems has stipulated an international cooperation of multiple disciplines such as physics, mathematics, electrical engineering, mechanical engineering and specialisms like control engineering and safety. By cooperation of these disciplines in a structured way, the ADEPT program provides a virtual research lab community from labs of European universities and industries [25].

REFERENCES

[1] M. R. Montgomery, "The urban transformation of the developing world," *Science*, vol. 319, no. 5864, pp. 761–764, 2008.

[2] D. Schrank, B. Eisele, and T. Lomax, "TTIs 2012 urban mobility report," *Texas A&M Transportation Institute. The Texas A&M University System*, 2012.

[3] W. Adams, Patent US 300 827 A, June 24, 1884.

[4] P. Albert L, Patent US 433 181 A, July 29, 1890.

[5] P. Edward B, Patent US 422 149 A, February 25, 1890.

[6] *Public Investment Criteria*. Studies in the Economic Development of India 4, London and Cambridge: Allen and Unwin and MIT Press, 1967.

[7] S. Buerger, B. Lohmann, M. Merz, B. Vogel-Heuser, and M. Hallmannsegger, "Multi-objective optimization of hybrid electric vehicles considering fuel consumption and dynamic performance," in *Vehicle Power and Propulsion Conference (VPPC), 2010 IEEE*. IEEE, 2010, pp. 1–6.

[8] R. Cook, A. Molina-Cristobal, G. Parks, C. O. Correa, and P. J. Clarkson, "Multi-objective optimisation of a hybrid electric vehicle: drive train and driving strategy," in *Evolutionary Multi-Criterion Optimization*. Springer, 2007, pp. 330–345.

[9] M. Gobbi, "A k, k-ε optimality selection based multi objective genetic algorithm with applications to vehicle engineering," *Optimization and Engineering*, vol. 14, no. 2, pp. 345–360, 2013.

[10] X. Xue, K. W. E. Cheng, T. W. Ng, and N. C. Cheung, "Multi-objective optimization design of in-wheel switched reluctance motors in electric vehicles," *Industrial Electronics, IEEE Transactions on*, vol. 57, no. 9, pp. 2980–2987, 2010.

[11] G. Mastinu and M. Ploechl, *Road and Off-Road Vehicle System Dynamics Handbook*. CRC Press, 2014.

[12] L. Guzzella and A. Sciarretta, *Vehicle propulsion systems*. Springer, 2007, vol. 1.

[13] T. J. Barlow, S. Latham, I. McCrae, P. Boulter *et al.*, *A reference book of driving cycles for use in the measurement of road vehicle emissions*, 2009, vol. 1, no. 1.

[14] M. Gobbi, F. Levi, and G. Mastinu, "Multi-objective stochastic optimisation of the suspension system of road vehicles," *Journal of sound and vibration*, vol. 298, no. 4, pp. 1055–1072, 2006.

[15] M. Gobbi, I. Haque, P. Papalambros, and G. Mastinu, "Optimization and integration of ground vehicle systems," *Vehicle System Dynamics*, vol. 43, no. 6-7, pp. 437–453, 2005.

[16] M. Pourabdollah, N. Murgovski, A. Grauers, and B. Egardt, "Optimal sizing of a parallel PHEV powertrain," *IEEE Transactions on Vehicular Technology*, vol. 62, no. 6, pp. 2469–2480, 2013.

[17] M. Eshani, Y. Gao, S. E. Gay, and A. Emadi, "Modern electric, hybrid electric and fuel cell vehicles," *Fundamentals, Theory, and Design. Boca Raton, FL: CRC*, 2005.

[18] G. Mastinu, M. Gobbi, and C. Miano, *Optimal Design of Complex Mechanical Systems: With Applications to Vehicle Engineering*. Springer, 2007.

[19] X. Wei, P. Pisu, G. Rizzoni, and S. Yurkovich, "Dynamic modeling of a hybrid electric drivetrain for fuel economy, performance and driveability evaluations," in *ASME 2003 international mechanical engineering congress and exposition*. American Society of Mechanical Engineers, 2003, pp. 443–450.

[20] G. Jing, M. Ouyang, and J. Li, "Vehicle Dynamic Simulation for Efficiency Optimization of Four-wheel Independent Driven Electric Vehicle," in *World Electric Vehicle Journal*. World Electric Vehicle Journal, 2010, pp. 319–324.

[21] P. Mellor, D. Roberts, and D. Turner, "Lumped parameter thermal model for electrical machines of TEFC design," in *IEE Proceedings B (Electric Power Applications)*, vol. 138, no. 5. IET, 1991, pp. 205–218.

[22] J. Meng, X. Wen, Y. Zhong, Z. Qiu, and L. Kong, "A thermal model for electrothermal simulation of power modules," in *Electrical Machines and Systems (ICEMS), 2013 International Conference on*. IEEE, 2013, pp. 1635–1638.

[23] D. Doerffel and S. A. Sharkh, "A critical review of using the Peukert equation for determining the remaining capacity of lead-acid and lithium-ion batteries," *Journal of Power Sources*, vol. 155, no. 2, pp. 395–400, 2006.

[24] M. Alexander, J. Allison, and P. Papalambros, "Decomposition-based design optimisation of electric vehicle powertrains using proper orthogonal decomposition," *International Journal of Powertrains*, vol. 1, no. 1, pp. 72–92, 2011.

[25] A. Stefanskyi, A. Dziechciarz, F. Chauvicourt, G. E. Sfakianakis, K. Ramakrishnan, K. Niyomsatian, M. Curti, N. Djukic, P. Romanazzi, S. Ayat, S. Wiedemann, W. Peng, and S. Stipetic, "Researchers within the EU funded Marie Curie ITN project ADEPT, grant number 607361," 2013-2017.